Planar tunneling spectroscopy of $Y_{1-x}Pr_xBa_2Cu_3O_7$ thin films as a function of crystallographic orientation

M. Covington* and L. H. Greene
Loomis Laboratory of Physics, University of Illinois at Urbana-Champaign, Urbana, Illinois 61801
(Received 21 September 1999; revised manuscript received 14 January 2000)

We present a systematic study of the charge transport and quasiparticle tunneling properties of $Y_{1-x}Pr_xBa_2Cu_3O_7$ thin films. Pr doping increases the resistivity along the copper oxide planes and suppresses the superconducting critical temperature T_c, ultimately inducing a superconductor-insulator transition. The tunneling conductance is reproducible and correlated with the crystallographic film orientation. The crystallographic dependence can be divided into two distinct categories: tunneling into (001)-oriented (c-axis) films and tunneling into (100)-, (110)-, and (103)-oriented (ab-oriented) films. c-axis tunneling data exhibit a conductance dip at zero bias and a broad temperature-dependent peak over $\sim 15-40$ mV that decreases in magnitude but stays fixed in energy for increasing Pr doping levels. ab-plane tunneling data exhibit a zero-bias conductance peak and a gaplike feature at an energy that scales roughly linearly with T_c for $x=0.0$, 0.2, and 0.4. When $x=0.5$, the resistivity is not linear in temperature and a zero-bias conductance dip is observed. The background conductance that ensures conservation of states in the low-temperature ab-plane data exhibits temperature- and doping-dependent structure over $\sim 15-40$ mV that is very similar to the peak observed in c-axis tunneling. Finally, analysis of the temperature and magnetic field dependence of the zero bias conductance peak indicates that states are conserved to within $\sim 20\%$, supporting its interpretation as a feature of a superconducting density of states.

I. INTRODUCTION

Tunneling spectroscopy is an experimental technique that provides the most direct measurement of the superconducting quasiparticle density of states,[1] probing the electronic structure near the Fermi energy with unsurpassed resolution. For temperatures much less than the superconducting critical temperature T_c, the conductance through a tunnel junction is roughly proportional to the superconducting quasiparticle density of states. Knowledge of the density of states enables one to predict thermodynamic properties below T_c, like the electronic specific heat. More importantly, tunneling spectroscopy allows detailed measurement of the superconducting gap and fine structure beyond the gap. In low-T_c superconductors, this fine structure provides unambiguous proof that the electron-phonon interaction is responsible for superconductivity, confirming the BCS hypothesis. By analogy, observation of similar structure in high-T_c superconductors can provide important information about the superconducting mechanism in the cuprates. Even the absence of this fine structure is important because it adds constraints to any microscopic theory purporting to describe high-T_c superconductivity.

Motivated by the past success of tunneling spectroscopy, numerous researchers have attempted to measure the density of states of the high-T_c superconductor $YBa_2Cu_3O_7$ (YBCO).[2–5] The first reproducible tunneling data came from planar junctions with conventional metal counterelectrodes. Very reproducible results were observed from both thin films and crystals and from different research groups. However, the data exhibit strikingly unconventional features, as shown in Fig. 1. Many experimental data indicate that the superconducting gap in YBCO has d-wave symmetry.[6] But the planar tunneling conductance only exhibits a weak gaplike structure around ~ 20 meV that resembles neither an s-wave nor a d-wave bulk superconducting gap. There are many more states within this gaplike structure even when compared to a d-wave gap. Nevertheless, this gaplike structure is intriguing because it appears near an energy where one expects to observe a superconducting gap, $eV \sim 2k_BT_c$.

Another interesting aspect of the tunneling conductance is its crystallographic dependence. When the tunneling current is predominantly directed perpendicular to the copper oxide planes, referred to as c-axis tunneling, the conductance exhibits a dip at zero bias and broadly peaked structure over $\sim 15-40$ meV. These data, however, are qualitatively different than the data measured when the tunneling current is predominantly directed parallel to the copper oxide planes. This will be referred to as ab-plane tunneling. In this geometry, the conductance exhibits a zero-bias conductance peak (ZBCP) and a gaplike feature (GLF) at ~ 16 meV.

Tunneling spectroscopy of cation-doped[7,8] and oxygen-deficient[9] YBCO has also been performed. These prior results are all from c-axis tunneling experiments. These data intriguingly show that, while the broad peak in the $\sim 15-40$ meV range in the c-axis data gets weaker with doping, it stays fixed in energy even though T_c is suppressed. The c-axis Pr-doped YBCO data presented in this article confirm previous data obtained from single crystals.[8] In contrast, the ab-plane GLF exhibits a markedly different doping dependence than that of the c axis. The energy of the ab-plane GLF decreases when Pr is doped into YBCO and T_c is consequently suppressed. Similar to the characteristics around zero bias, the T_c dependence of the peaklike structures also exhibits crystallographic anisotropy.

In this article, the charge transport and planar tunneling

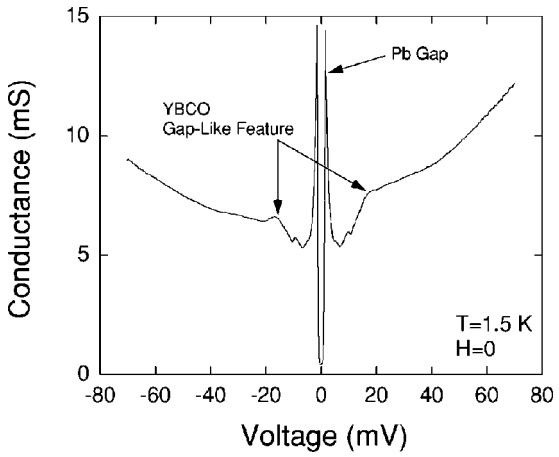

FIG. 1. Typical data from an ab-oriented-YBCO/Pb planar tunnel junction illustrating the contrasting gap structure from YBCO and Pb. The temperature is well below the T_c of both YBCO and Pb. The Pb gap at 1.35 mV and the Pb phonon structure at 8 and 10 mV are clearly observed. The decrease in conductance at approximately 17 mV is the YBCO gaplike feature (GLF). Note that the subgap conductance of the YBCO GLF is much greater than that of the Pb gap. Other than the Pb density of states, there is no resemblance between these data and that expected when tunneling between two conventional superconductors.

conductance properties of $Y_{1-x}Pr_xBa_2Cu_3O_7$ (YPBCO) thin films are presented. This article also includes a further analysis of the temperature and magnetic field dependence of the ZBCP from YBCO/Cu tunnel junctions reported in Ref. 10. A brief summary of the theoretical predictions for a *d*-wave symmetry superconducting order parameter at a surface is given in Sec. II. The experimental details of thin film growth, measurement of the resistivity, and tunnel junction fabrication and measurement are discussed in Sec. III. The experimental YPBCO resistivity data are shown in Sec. IV. The crystallographic and doping dependence of the YPBCO tunneling conductance is presented in Sec. V. A discussion of the background normalization that leads to conservation of states in the ab-plane data will be presented in Sec. VI. A further analysis of the temperature and magnetic field dependence of the zero-bias conductance peaks is presented in Sec. VII. Finally, concluding remarks are stated in Sec. VIII.

II. THEORETICAL BACKGROUND

A background discussion of the tunneling spectroscopy of *d*-wave superconductors and the impact of surfaces will be given first. This will briefly summarize the physics of unconventional superfluids in general[11] and *d*-wave symmetry superconductors in particular[12–17] at surfaces, and the consequent formation of Andreev bound states, as developed in previously published articles.

Anisotropic superconductors differ from conventional superconductors by the phase and amplitude variations of the order parameter across the Fermi surface. This leads to markedly different behavior between the two at surfaces and interfaces. Specifically, when the node of a *d*-wave order parameter is normal to a specularly reflecting surface, normal reflection at the surface leads to strong Andreev reflection. This happens at a (110)-oriented surface for a

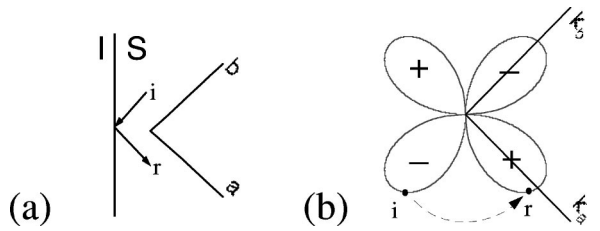

FIG. 2. Schematic illustration of specular quasiparticle reflection at a (110)-oriented surface of a superconductor with a $d_{x^2-y^2}$-symmetry order parameter. (a) Configuration space. The classical trajectory of a quasiparticle incident on a superconductor-insulator interface is indicated by the arrow labeled *i*. This quasiparticle is specularly reflected into another quasiparticle state whose trajectory is indicated by the arrow labeled *r*. The YBCO *a* and *b* crystallographic directions are also shown. (b) Momentum space. The sign and amplitude of the order parameter for the quasiparticle states corresponding to (a) are shown. The incident quasiparticle is in a state where the gap is equal to $-|\Delta_i|$. This quasiparticle is then reflected, represented by the dashed line, into a state where the gap is equal to $+|\Delta_r|$.

$d_{x^2-y^2}$-symmetry order parameter and is shown in Figs. 2(a) and 2(b). A quasiparticle incident on the superconductor-insulator interface experiences a gap of $-|\Delta_i|$ along its classical trajectory. This quasiparticle is then reflected into a state where the gap is equal to $+|\Delta_r|$. Hence, the quasiparticle experiences a change in the sign of the order parameter along its trajectory. This leads to strong Andreev reflection, where an electronlike (holelike) quasiparticle is retroreflected into a holelike (electronlike) state.[18] This combination of normal and Andreev scattering results in the formation of quasiparticle bound states at the surface.

The most relevant class of bound states is composed of those formed from spatially localized, evanescent waves with energies below the superconducting gap, $E<\Delta$. While these states are forbidden in a clean bulk material, they can exist at a surface. The energy of these states is set by the boundary condition at the surface, where the superconducting pair potential is effectively odd in configuration space. The only possible solution is a state at zero energy.[19] This is a very robust result that leads to substantial spectral weight in the density of states at the Fermi energy. Only perfectly specular (100)- or (010)-oriented surfaces have no bound states. All other surface orientations between (100) and (110) will have at least some quasiparticle trajectories that experience a change in the sign of the order parameter and, hence, a zero-energy bound state will form. Quasiparticle states above the gap will also form bound states and geometrical resonances, but these contribute very little spectral weight to the density of states and will hereafter be ignored.

This mixing of electron and hole states at the surface also impacts the amplitude of the order parameter. Self-consistent calculations predict substantial pair breaking near the surface in the presence of this strong Andreev scattering. For the particular case of a $d_{x^2-y^2}$-symmetry order parameter at a specular (110)-oriented surface, the pair potential is suppressed entirely to zero at the interface. Hence, a fully formed $d_{x^2-y^2}$ gap is possible only at a specular (100)-oriented surface. All other orientations will have at least some pair breaking and extra states within the gap.

The Andreev bound state will shift to finite energy in the

presence of superfluid flow by an amount given by $v_F p_s \sin(\phi_c)$ (where v_F is the Fermi velocity, p_s is the superfluid momentum, and ϕ_c is the tunneling cone). This is the usual Doppler shift of the quasiparticle energy. The shift in energy is positive (negative) for quasiparticles moving in the same (opposite) direction as p_s. A finite superfluid momentum can occur in at least two different ways. Either an external magnetic field can induce the circulation of Cooper pairs or the superfluid can spontaneously circulate in zero field when two order parameters with a relative $\pi/2$ phase difference coexist. In the latter case, the gradient in phase between the two order parameters drives the superfluid circulation.

Finally, these Andreev bound states are different from localized states that originate from spatial variations in a Hartree-Fock potential. Since Andreev bound states exchange charge with the superconducting condensate by Andreev reflection, they can carry current even though they are localized in space. Hence, they will appear as a zero-bias conductance peak in a tunneling experiment.

III. EXPERIMENTAL DETAILS

A. Thin film growth

In this experiment, YPBCO thin films are studied with Pr concentrations of $x=0.0$, 0.2, 0.4, 0.5, and 1.0. Tunneling measurements are performed for all four film orientations, but only on superconducting films where $x=0.0-0.5$. The resistivity is measured for all five doping levels, but only the results from (001)-oriented films are shown. The films are grown by off-axis magnetron sputter deposition from single stoichiometric targets.[20,21] (001)- and (103)-oriented films are grown directly onto the substrate while (100)- and (110)-oriented films employ a $PrBa_2Cu_3O_7$ (PBCO) template. Curiously, YPBCO with $x>0$ will not follow the orientation of (100)- and (110)-oriented PBCO templates but will follow the orientation of an undoped YBCO layer grown on top of a PBCO template. Therefore, all of the tunneling results on (100)- and (110)-oriented YPBCO films are from such trilayers. This structure is beneficial to tunneling measurements because it eliminates film resistance below 90 K and enables the measurement of the tunneling conductance above the T_c of YPBCO. However, it is exceedingly difficult to measure the T_c of the YPBCO layers in such a heterostructure and their T_c's are unknown. It will be assumed that the T_c's of (100)- and (110)-oriented YPBCO layers are the same as comparable (001)- and (103)-oriented films, which is true for undoped YBCO. Finally, x-ray diffraction and scanning electron microscopic analysis reveals no significant structural differences between different doping levels.

B. Resistivity measurements

The resistivity is measured with two conventional four-probe geometries. In the first method, current and voltage contacts are painted parallel to each other across the film surface with Ag paint. This method is the most commonly used. In the second method, conventional photolithography is used to pattern a ~ 2 mm long and 100 mm wide bar with current and voltage contacts. The results from these two measurement techniques are consistent with each other and in agreement with other published data.

The films studied in these experiments exhibit zero resistance superconducting transition temperatures of 90, 70, 45, and 20 K for Pr concentrations of $x=0.0$, 0.2, 0.4, and 0.5, respectively. PBCO, $x=1.0$, films are insulating and exhibit variable range hopping behavior[22] below ~ 120 K. The homogeneity of the superconducting films is verified by magnetic susceptibility measurements. These films reproducibly exhibit an onset to diamagnetic screening at the same temperature in which they exhibit zero resistance. Single superconducting transitions are observed in both the resistivity and the susceptibility. The transitions in the resistivity and susceptibility both get broader, in temperature, with increasing Pr concentration, with the transition widths being comparable for the two measurements. Undoped YBCO films typically exhibit ~ 1 K transition widths while YPBCO films have ~ 10 K transition widths when $x=0.5$.

C. Junction fabrication and measurement

There are two methods of tunnel junction fabrication. In the first and most widely used method, Pb counterelectrodes are evaporated *ex situ* directly onto the YPBCO film surface.[5,21] The junction area is typically on the order of 0.1 mm^2. This technique relies upon the reaction of the two materials to form an insulating tunnel barrier. The microscopic nature and chemical composition of the insulator are largely unknown. But there are two measures of the barrier thickness. First, the parabolic background conductance of undoped ab-oriented YBCO can be fit to a model of an asymmetrically shaped trapezoidal insulating barrier,[23] yielding a barrier thickness of approximately 30 Å. Second, grazing incidence x-ray diffractometry of c-axis-YBCO/Pb films[24] indicates that the barrier thickness is a few tens of angstroms.

The second method of junction fabrication was used for the junctions reported in Ref. 10. It employs a monolayer of rodlike molecules, ~ 20 Å long, that spontaneously adsorb onto the YBCO surface, forming a densely packed self-assembled monolayer. Similar molecular monolayers can be routinely formed on metal surfaces, like Au.[25] The molecules used in this experiment are tailored to bond to the exposed Cu atoms on the YBCO surface.[26] After the YBCO films are grown, they are soaked *ex situ* for 2 days in a dilute solution of 1,12 diaminododecane and acetonitrile, whereby the monolayer is formed. A metallic counterelectrode is subsequently evaporated through a stainless steel shadow mask.

A film with a set of junctions is mounted on a variable temperature probe for measurement. The junction resistance is measured with a conventional four-probe geometry. Both dc and ac tunneling measurements are performed as a function of temperature and magnetic field.

IV. YPBCO RESISTIVITY

The resistivity of Pr-doped YBCO exhibits very rich and complex behavior, as shown in Fig. 3(a). These data are comparable to other published work.[27–29] Pr doping increases the resistivity along the planes and suppresses T_c. In addition, Pr doping induces features in the ab-plane resistivity that are characteristic of both planar and chain dopants in YBCO.

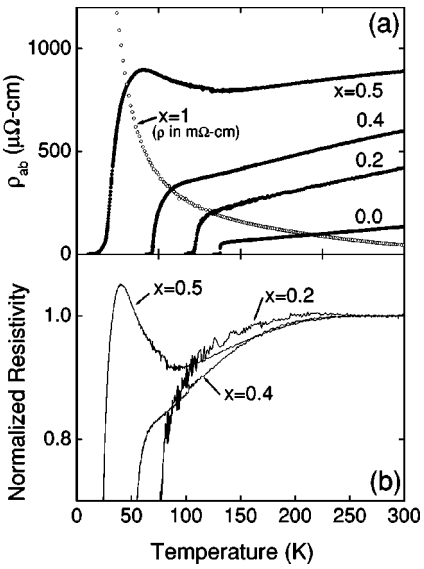

FIG. 3. (a) Resistivity along the copper oxide planes, ρ_{ab}, for (001)-oriented $Y_{1-x}Pr_xBa_2Cu_3O_7$ thin films. Doping YBCO with Pr increases the resistivity and suppresses T_c. Note the substantial extrapolated zero temperature residual resistivity and the S-shaped curvature which develops with increasing Pr doping levels. (b) Illustration of the characteristic underdoped curvature in the Pr-doped YBCO resistivity. The resistivity data for $x=0.2-0.5$ are normalized by a linear function, as described in the text.

The first feature of Pr doping is the development of a significantly large extrapolated zero temperature resistivity. This is characteristic of disorder within the copper oxide planes which, as an example, occurs when Zn is substituted for Cu.[30–32] Planar doping introduces a substantial residual resistivity while the slope $d\rho/dT$ stays roughly constant. By analogy to the behavior of conventional metals, this suggests that pure planar doping introduces scattering within the planes without affecting the carrier concentration.

The second feature of Pr doping is the development of S-shaped curvature in the resistivity. This is characteristic of either oxygen depletion[33] or cation substitutions for chain Cu atoms.[34,35] Pure chain doping leads to a resistivity with an increased slope and S-shaped curvature while still extrapolating to at or below zero at zero temperature. Again, by analogy to conventional metals, the increase in the slope while still extrapolating to zero is an indication of a reduction in the number of charge carriers within the planes without any increase in carrier scattering. The S-shaped curvature deviates from the linear temperature dependence exhibited by optimally doped YBCO and is postulated to be correlated with the opening of the spin gap in underdoped cuprates.[33]

Therefore, YPBCO is very similar to underdoped YBCO with planar disorder; i.e., the development of a significant residual resistivity accompanies the change in the slope and shape of the resistivity.[31,32] The S-shaped curvature is more difficult to observe than the residual resistivity. To highlight this curvature, the superconducting YPBCO data with $x>0$ are normalized by a linear function. The data from Fig. 3(a) are fit between 250 and 300 K, normalized by this linear function, and plotted in Fig. 3(b). The downward deviation from linearity is a common feature observed in the resistivity of all underdoped cuprates. The doping dependence of the slope, however, differs from the simple monotonic behavior

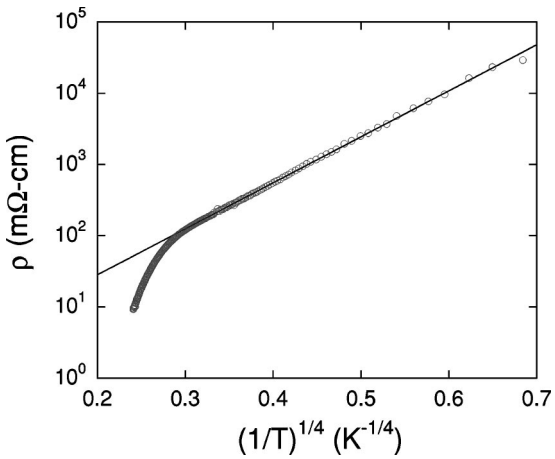

FIG. 4. Temperature-dependent resistivity of the PBCO film shown in Fig. 3(a) plotted as $\log(\rho)$ vs $1/T^{1/4}$ to illustrate the variable range hopping transport. The line is a linear fit to the data between 0.3 and 0.7 $K^{-1/4}$.

typically observed in underdoped cuprates. The slope shows an initial increase from $x=0.0$ to 0.2, but then decreases as x goes to 0.4 and 0.5. For reference, the slopes of the linear fits are 0.83, 1.46, 1.14, and 0.31 $\mu\Omega$ cm/K for $x=0.0$, 0.2, 0.4, and 0.5, respectively.

Another significant feature of the YPBCO resistivity is the evidence for carrier localization around the Fermi energy for large Pr concentrations. The $x=0.5$ data exhibit metallic behavior, $\delta\rho/\delta T>0$, above approximately 100 K. But the slope changes sign below 100 K, and the resistivity displays insulating behavior, $\delta\rho/\delta T<0$, before superconducting. This foreshadows the insulating state of pure PBCO, which exhibits a temperature dependence characteristic of variable range hopping transport.[22] This is shown in Fig. 4. The change in slope around 0.3 $K^{-1/4}$, which corresponds to a temperature of roughly 120 K, is a characteristic feature of PBCO films that are fully oxygenated.[36] This lends support to the assumption that the YPBCO films are fully oxygenated for all the Pr concentrations studied.

Finally, these YPBCO films exhibit a superconductor-insulator transition when the sheet resistance per copper oxide bilayer is $\sim$ 7 k$\Omega/\square$. This is close to the quantum resistance for Cooper pairs, $R_Q=h/(2e)^2\sim 6.45$ kΩ. Such a crossover is also observed in oxygen-deficient Zn-doped YBCO thin films[31] and single crystals.[32] However, while the sheet resistance per copper oxide bilayer sets the crossover in thin films, the sheet resistance per individual copper oxide layer appears to set the criterion in single crystals. One possible reconciliation is the additional grain and twin boundary scattering of thin films that additively contributes to the resistivity. Nevertheless, the YPBCO sheet resistance, either per copper oxide layer or bilayer, is at least as large as R_Q when the superconductor-insulator transition is reached.

V. TUNNELING: CRYSTALLOGRAPHIC AND DOPING DEPENDENCE

A. Junction analysis and characterization

The first measurement of every junction involves the characterization of the current to verify that elastic tunneling

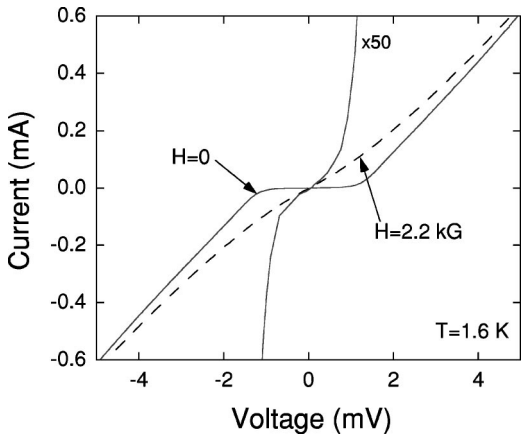

FIG. 5. Data from a (001)-oriented $Y_{0.6}Pr_{0.4}Ba_2Cu_3O_7$/Pb planar tunnel junction showing how leakage current is determined. The solid lines represent data taken with the Pb electrode in its superconducting state, and the dashed line represents data taken when Pb is normal. The data where Pb is superconducting are plotted according to both the indicated current scale and with the current scale magnified by a factor of 50. This particular junction exhibits ~2% leakage current, as discussed in the text.

is the dominant transport process. A junction is a useful spectroscopic device only when elastic tunneling dominates over all other possible transport processes. When this condition is satisfied, the tunneling conductance between a normal metal and a superconductor is a measure of the superconducting density of states. Since YPBCO is a new material with a density of states that is *a priori* unknown, a Pb counterelectrode is used for the following three reasons. First, the Pb superconducting density of states is well known and it is used as a diagnostic to determine the amount of elastic tunneling current through the junction. Second, Pb has a T_c of 7.2 K, which makes it convenient to study at the temperatures achieved in a simple ^{4}He cryostat. Third, Pb forms good insulating tunnel barriers when evaporated onto YPBCO.

The Pb superconducting density of states is observed in all of the YPBCO/Pb junctions reported in this article. The Pb gap appears at 1.35 meV and the Pb phonon structure appears at ~8 and ~10 meV, indicating that inelastic tunneling processes can be excluded from consideration in this energy range. These features are clearly seen in Fig. 1 and are representative of the structure routinely observed. These features disappear when Pb is driven normal, either by temperature or magnetic field. The amount of nontunneling current through the junction is determined by measuring the conductance at zero bias well below 7.2 K with the Pb electrode in its superconducting and normal state. The Pb gap strongly suppresses the zero-bias current below its normal-state value, as shown in Fig. 5. When Pb is superconducting, the zero-bias conductance of this junction is 50 times smaller than its normal-state value. This ratio should be $\sim 10^4$ for a perfect junction with only elastic tunneling present. Therefore, ~2% of the current through this particular junction originates from transport processes other than elastic tunneling. In general, this value of the leakage current is strictly valid only at zero bias, with the Pb electrode in its superconducting state, and at the measured temperature. Even when a high-quality Pb gap is observed, other transport processes, like hopping transport, can occur either at high bias or at higher temperature. In fact, we cannot exclude the possibility of hopping transport in some of the data presented in this article. However, the voltage where hopping may occur is beyond the energies of the ZBCP and GLF. So it has a minimal impact on our results and conclusions.

For junctions with Pb counterelectrodes, only those junctions that exhibit a well-defined Pb superconducting density of states along with other signatures of elastic tunneling are presented. Leakage current, as defined in Fig. 4, ranges from 1% to 23%. The strength and energy of the YPBCO features are independent of the amount of leakage current. This proves they originate from elastic tunneling current rather than other transport processes responsible for the leakage.

The characterization of the current through the YBCO/Cu junctions is more difficult because Cu is nonsuperconducting with a featureless density of states. Even though the amount of leakage current cannot be quantified, the sum of the experimental observations indicates that the current through the YBCO/Cu junctions, like the YBCO/Pb junctions, is dominated by elastic tunneling current.[10]

The remaining tunneling data shown below have the Pb counterelectrode driven normal either by temperature or magnetic field. Hereafter, we will assume that the tunneling conductance can be expressed as a convolution of the square of the modulus of the tunneling matrix element, the densities of states of YPBCO and Pb, and the derivative of the Fermi function with respect to voltage.[37] This follows from modeling the tunneling current with the Fermi golden rule which states that the conductance through an NIS tunnel junction is given by

$$G_{NIS} = G_{NIN'} \int_{-\infty}^{\infty} N_S(E) \frac{\delta f(E-eV)}{\delta V} dE. \qquad (1)$$

Here $G_{NIN'}$ is the tunneling conductance with both electrodes normal, $N_S(E)$ is the YPBCO density of states relative to its normal state value, and $f(E-eV)$ is the Fermi function. $G_{NIN'}$ includes the tunneling matrix element and the normal density of states of YPBCO and the counterelectrode.

Finally, all of the tunneling data presented in this article are highly reproducible. The data presented for a particular doping level and crystallographic direction are representative of all the data from that specific Pr concentration and tunneling direction. The voltage across the junction is defined to be that of the Pb electrode with respect to the YPBCO electrode.

B. Crystallographic dependence

YPBCO, like other high-T_c superconductors, has a very anisotropic crystal structure. As a consequence, YPBCO has a corresponding anisotropy in its electronic properties. This is studied by tunneling into thin films with different crystallographic orientations. The data in this article are reproducible and can be classified into two distinct categories: *c*-axis and *ab*-plane tunneling. *c*-axis tunneling refers to tunnel junctions fabricated on (001)-oriented films, where the tunneling current is predominantly directed perpendicular to the copper oxide planes. *ab*-plane tunneling refers to junctions

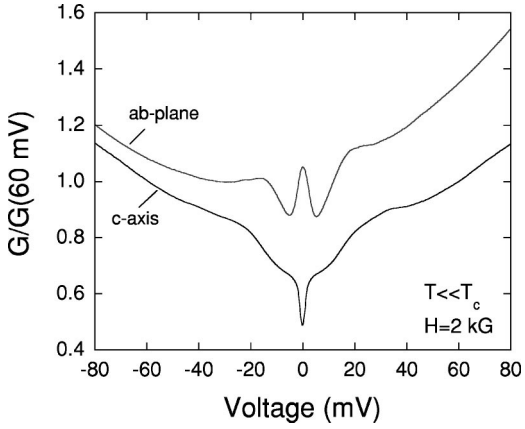

FIG. 6. Crystallographic dependence of the planar YBCO tunneling conductance. Qualitative differences are observed between *ab*-plane and *c*-axis tunneling. *ab*-plane data exhibit a zero-bias conductance peak (ZBCP) and a gaplike feature (GLF) at approximately 17 mV. *c*-axis data exhibit a conductance dip at zero bias and a broad peaklike structure that is different from the *ab*-plane GLF, as discussed in the text.

fabricated on (100)-, (110)-, and (103)-oriented films, where the current is predominantly directed parallel to the copper oxide planes. For both tunneling geometries, only slight differences in the conductance are observed from junction to junction, such as the detailed shape of the background and the strength of the features that appear below ~40 mV. For *ab*-plane tunneling, the differences in the tunneling characteristics between junctions fabricated on films with different orientations are consistent with the differences between junctions fabricated on films with the same orientation. Given this empirical observation, the data from all three *ab*-plane orientations will be considered equivalent.

In Fig. 6, typical data from undoped *ab*-oriented and *c*-axis YBCO films are presented side by side to illustrate the differences between the two orientations. There are three specific distinctions reproducibly observed. First, at zero bias a conductance peak is observed in the *ab*-plane data while a conductance dip is observed in the *c*-axis data. Second, there are subtle differences in the peaks appearing at ~20 mV. The peak in the *ab*-plane data is reproducibly observed at around ~16 mV, which is less than the ~22 mV value of the *c*-axis peak. This difference has also been noticed by others.[4] Third, the voltage dependence for the two orientations is different at voltages beyond those plotted in Fig. 6. *ab*-plane data exhibit a parabolic background conductance that is typical of the behavior observed in planar metal/oxide/metal tunnel junctions. This can be described with an asymmetric, trapezoidally shaped potential barrier separating the two electrodes.[23] *c*-axis data exhibit a background conductance that varies linearly with voltage. There has been much interest and speculation over the origin of this behavior,[38–40] but this subject is beyond the scope of this paper and we will omit any further discussion on this point.

There are three exceptions to the observed crystallographic dependence. First, *ab*-plane tunneling features are observed from nominally *c*-axis films, which have more than 50% of the surface covered by *a*-axis grains. Second, *ab*-plane films etched with a dilute solution of Br in methanol (1:100 by volume) exhibit *c*-axis tunneling features. Third, *ab*-plane tunneling features are observed when tunneling into *c*-axis films modified with a self-assembled monolayer. The first behavior is understandable since the surface area of the *a*-axis grains is greater than that of the underlying *c*-axis film. The resistance for *ab*-plane tunneling will then be less than for *c*-axis tunneling and dominate the junction resistance. The second behavior is unexpected. We propose that, since the Br etch rate is much faster in the *ab*-plane direction than in the *c*-axis direction,[41] the exposed planes of the *ab*-oriented films are rapidly and inhomogeneously etched. The pitted surface exposes an effectively large area for *c*-axis tunneling and possibly a thicker tunnel barrier in the *ab*-plane direction, consequently leading to preferential tunneling along the *c* axis. For the third behavior, there is indirect evidence for interdiffusion of the counterelectrode through the self-assembled monolayer and into the YBCO film,[10,42] thereby opening up *ab*-plane tunneling channels in a globally oriented *c*-axis film.

C. Doping dependence

The effect of Pr doping, and the concomitant T_c reduction, is studied by measuring films with different Pr concentrations. Some YPBCO tunneling measurements with $x>0$ are performed on YPBCO layers, a few hundred angstroms thick, grown on top of an undoped YBCO layer. As mentioned above, this layering is necessary to achieve the proper orientation for (100)- and (110)-oriented YPBCO. But it is also found that junctions fabricated on (103)- and (001)-oriented YBCO/YPBCO bilayers exhibit less leakage current than junctions fabricated on single layer YPBCO films. The same features are observed in the conductance for single layer YPBCO and bilayer YBCO/YPBCO films, so proximity effects can be excluded.

The dependence of the *ab*-plane and *c*-axis YPBCO tunneling conductance is shown in Figs. 7(a) and 7(b), respectively. Both the *ab*-plane and *c*-axis data are normalized by the value of the conductance at +60 mV so that they can fit on the same plot. The conductance at 60 mV is 0.74, 229, 263, and 340 mS for the $x=0.0$, 0.2, 0.4, and 0.5 *ab*-plane data, respectively. The conductance at 60 mV is 181, 34, 208, and 54 mS for the $x=0.0$, 0.2, 0.4, and 0.5 *c*-axis data, respectively. As observed in Fig. 7, the *ab*-plane conductance data for $x=0.0-0.4$ and the *c*-axis conductance data for $x=0.0-0.5$ strikingly maintain the same characteristic features for the particular crystallographic orientation. In addition, Pr doping weakens the strength of these features. However, the reproducibility of these features supports their interpretation as intrinsic features of the YPBCO electrode, despite their small size.

For *ab*-plane tunneling, a zero-bias conductance peak and gaplike feature are observed for $x=0.0-0.4$. Pr doping reduces the ZBCP height. Likewise, the depth of the GLF decreases with increasing Pr concentration. However, in contrast to the ZBCP, which is very pronounced for all three doping levels, the GLF becomes very subtle with higher doping levels. Yet a close inspection reveals that there is a distinct downward deviation from the background conductance for $x=0.0$, 0.2, and 0.4. It is also found that there is a clear

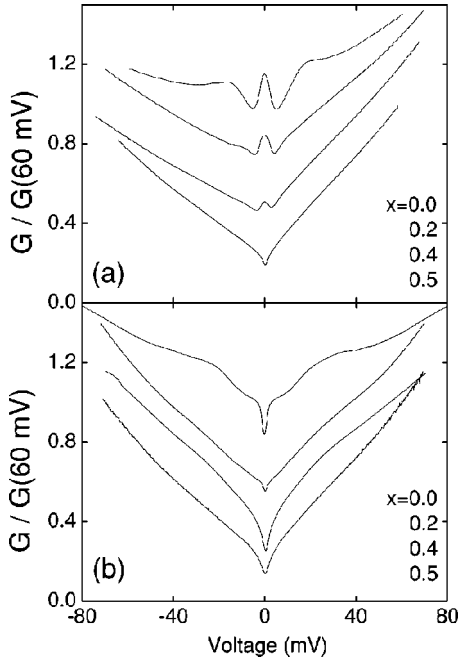

FIG. 7. Doping dependence of the YPBCO/Pb tunneling conductance. For both figures, the Pr concentration increases from top to bottom, as indicated. (a) Dependence of the ab-plane YPBCO conductance on Pr concentration. Note that the ZBCP and GLF are reproducibly observed for Pr concentrations between $x=0.0$ and $x=0.4$. The data are measured at either 4.2 K or 1.5 K. A magnetic field of 2 kG is also applied to drive the Pb electrode normal. The normalization values are listed in the text and the data for $x<0.5$ are shifted vertically for clarity. (b) Dependence of the c-axis YPBCO conductance on Pr concentration. Note that a dip in the conductance is always observed at zero bias. All the data are taken at 1.5 K in a 2 kG magnetic field. The normalization values are listed in the text and the data for $x<0.5$ are shifted vertically for clarity.

decrease in the energy where this GLF appears with decreasing T_c. Numerical derivatives of the conductance confirm this reproducible behavior.

For c-axis tunneling, a conductance dip and broadly peaked structure over $\sim 15-40$ mV is observed. These c-axis data are an independent confirmation of previously published data from Pr-doped YBCO single crystals.[8] These data also resemble the c-axis conductance when tunneling into oxygen deficient YBCO (Ref. 9) and YBCO doped with Al, Fe, Zn, and Gd.[7] This broad structure in the c-axis conductance behaves differently than the GLF observed in ab-plane tunneling. While the c-axis peak gets weaker with increasing Pr concentration, it exhibits no clear downward shift in energy as T_c is suppressed.

As shown in Fig. 7(a), the ab-plane tunneling conductance exhibits a qualitative change when the Pr concentration increases from 0.4 to 0.5. These data are also reproducible. Instead of a ZBCP, a conductance dip is observed at zero bias. Furthermore, a gaplike feature cannot be resolved. At first glance, the $x=0.5$ ab-plane data bear close resemblance to the c-axis tunneling data for the same Pr doping level. However, there are two specific differences that suggest the ab-plane and c-axis data are still different. First, the ab-plane background conductance is more asymmetric than the c-axis data and follows the same asymmetric trend established by the lighter doping levels. Second, the width of the

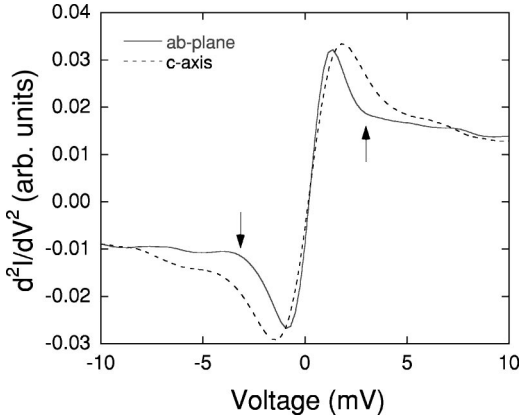

FIG. 8. Numerical derivatives of the ab-plane and c-axis conductance from $Y_{0.5}Pr_{0.5}Ba_2Cu_3O_7$. The conductance for each junction is shown in Fig. 7. Both junctions are measured at the same temperature and magnetic field of 1.5 K and 2 kG, respectively. The dip in the conductance around zero bias appears in the derivative as the curvature indicated by the arrows. The width, in energy, of the dip in the ab-plane data is reproducibly narrower than the dip in the c-axis data.

ab-plane conductance dip is narrower, in energy, than the c-axis dip. This is shown in Fig 8. The dip around zero bias manifests itself as the deviation from roughly linear behavior in dG/dV and is indicated by the arrows.

The physical origin for this zero bias dip is unknown. However, the disappearance of the ZBCP coincides with the appearance of localization in the ab-plane resistivity. This suggests that carrier localization is suppressing the formation of Andreev bound states. If so, the spatial extent of the localized states must be less than the superconducting coherence length, which sets the scale over which the constructive interference occurs. The localization length is difficult to extract from the $x=0.5$ data because there is no charge transport model that is applicable to the resistivity. Nevertheless, the localization length in insulating YPBCO with $x=0.63$ (Ref. 43) and PBCO (Ref. 44) has been estimated to be $\sim$15-20 Å and $\sim$85 Å, respectively. So spatially localized states extending on the order of the coherence length are at least plausible when $x=0.5$.

A more speculative explanation for the absence of the ZBCP is that the superconducting order parameter has s-wave symmetry when $x=0.5$. However, many materials issues must be addressed before such a conclusion can be made. The most definitive experiment would be a superconducting quantum interference device (SQUID) interferometry experiment like that used to determine the pairing symmetry of undoped YBCO.[6]

VI. TUNNELING: NORMALIZATION OF THE LOW-TEMPERATURE ab-PLANE DATA

A. Calculation of the normal-state background

Traditionally, either of two methods are used to empirically measure the normal-state background conductance. The first is to drive the superconductor normal with a magnetic field. This method is advantageous because the superconducting and normal-state conductance can be measured at the same temperature, i.e., with an equivalent Fermi distribution

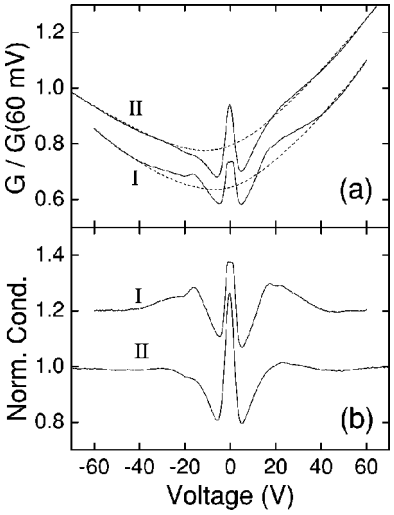

FIG. 9. Illustration of the nonconservation of states from undoped-YBCO/Pb junctions when the low-temperature conductance is normalized by the conductance measured at T_c. (a) Unnormalized data. The solid lines represent the conductance measured well below T_c and the dotted lines indicate the conductance measured at T_c. The data are normalized by the value of the conductance at 60 mV and the data labeled II are shifted vertically for clarity. (b) Normalized data. The normalized conductance from undoped YBCO typically exhibits too many states, as shown in the top curve labeled I. However, the normalized conductance occasionally exhibits too few states, as evident in the bottom curve labeled II. The top curve is shifted vertically by 0.2 for clarity.

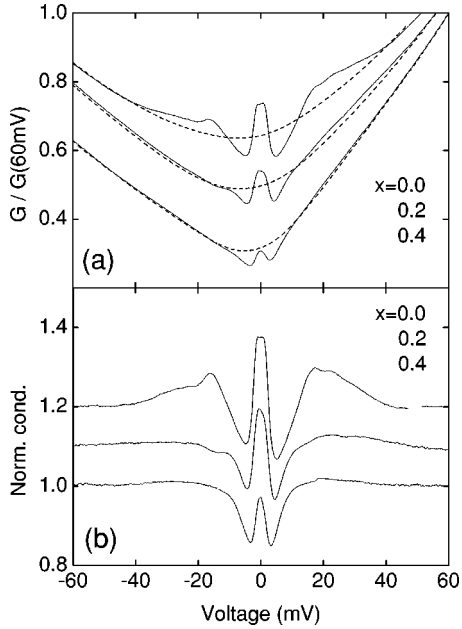

FIG. 10. Illustration of the nonconservation of states from Pr-doped-YBCO/Pb junctions when the low-temperature conductance is normalized by the conductance measured at T_c. (a) Unnormalized data. The solid lines represent the low-temperature data taken well below T_c and the dotted lines represent the conductance measured at T_c. The data are normalized by the value of the conductance at 60 mV and shifted vertically for clarity. (b) Normalized data. The normalized data from YPBCO films exhibit too many states when $x=0.0$ and 0.2, but they exhibit too few states when $x=0.4$.

of quasiparticles in the electrodes. This, however, is impractical for YPBCO because its upper critical field is on the order of 100 T, which is extremely difficult to achieve for any sustained period of time. The second method is to drive the superconductor normal with temperature. This method is easily achieved with planar tunnel junctions, which display excellent stability with varying temperature. In contrast, this method results in a normal-state background with greater thermal broadening than the low-temperature data.

However, there are additional complications with this latter method specific to the YPBCO junctions reported in this article. When the low-temperature data are normalized by the data measured at T_c, the normalized conductance exhibits either too many or too few states. Examples of this behavior are plotted in Figs. 9 and 10. Too many states are typically observed in the normalized conductance of YPBCO junctions with $x=0.0$ and 0.2. Too few states are observed in junctions where $x=0.4$. Note that the superconducting and normal conductances match at high bias, as expected when probing the density of states far beyond the gap. The nonconservation of states originates from the behavior around zero bias.

Hence, the dilemma: the Pb superconducting density of states is observed in the low-temperature conductance, indicating the dominance of elastic tunneling. In addition, the qualitative behavior of the ZBCP and GLF is consistent with a *d*-wave superconducting density of states. But the nonconservation of states in the normalized data is inconsistent with a superconducting density of states. However, because the *ab*-plane data so closely resemble a *d*-wave density of states, we instead hypothesize that the normal-state background is temperature dependent and proceed to numerically calculate a background conductance that conserves states.

The simplest way to numerically calculate a normal-state background is to fit the experimental conductance to a simple function, like a parabola or a linear function. This fit is done at high voltage and then extrapolated to the region around zero bias. However, the YPBCO background exhibits a nontrivial voltage dependence, which cannot be adequately fit by a simple function.

An alternative method is used, which will now be discussed. The key concept of the numerical procedure is that the superconducting conductance and the normal-state conductance, from the same temperature, will match if convolved with enough thermal broadening. This is a consequence of the conservation of states between the superconducting and normal states, and it occurs when thermal broadening washes out all features related to the superconducting density of states. So a procedure is developed whereby the experimental low-temperature *ab*-plane tunneling data are numerically convolved with hypothetical thermal broadening at a much higher temperature T_{conv}. This is just a simple numerical integration along the lines of the Fermi golden rule given in Eq. (1). This thermal broadening is then deconvolved from the convolved data using parameters that yield a smoothly varying background conductance. The deconvolution procedure employs fast Fourier transforms. Since there is no phase information, there are many different functions that can be extracted from the deconvolution. This is why the deconvolved data do not match the original low-temperature data. But the deconvolution proce-

dure is accurate because when the deconvolved data are ''reconvolved,'' the data match the original convolved data. The smoothly varying background is arguably the most plausible from a physical standpoint since fast oscillations with respect to voltage are unexpected from the tunneling matrix element and the normal density of states. Therefore, we propose that the low-temperature normal-state background calculated in this manner is a very good approximation of the actual background.

As a proof a concept, this convolution-deconvolution procedure is applied to both a parabolic background conductance and a hypothetical BCS density of states superimposed on this parabolic normal-state background. After going through this convolution-deconvolution procedure, the numerically calculated background matches the original parabolic background to better than 1%. Next, the BCS density of states plus parabolic background is used to numerically generate a background conductance. This hypothetical BCS conductance is convolved with a temperature well above that in which features related to the gap and inverse square-root singularity at the gap edge are no longer resolved. The deconvolved conductance matches the original parabolic background to within a few percent. In addition, the normalized data agree to within a few percent of the original BCS density of states. There is improved agreement when broadening is introduced in the BCS density of states via a phenomenological pair-breaking factor,[45] which is more applicable to the weak features in the YPBCO conductance.

Finally, we do not wish to emphasize the details of the numerical procedure any more than necessary. The numerical procedure discussed above is simply one of many ways of calculating a background conductance. We only want to present these numerically calculated backgrounds as being physically plausible, given our hypothesis of a temperature-dependent background. Most importantly, we stress that these backgrounds are calculated in the least-biased manner possible. This numerical procedure works well at impartially calculating a background conductance that conserves states.

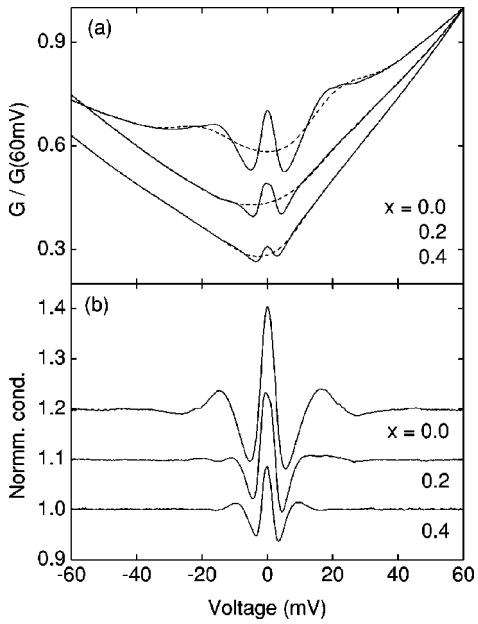

FIG. 11. Normalization of the ab-plane conductance using a numerically calculated background conductance that conserves states, as described in the text. (a) The low-temperature conductance is represented by a solid line and the background conductance is represented by a dotted line. The Pr concentration increases for each curve from top to bottom, as indicated. (b) Normalized data. The GLF energy decreases with decreasing T_c. Also, the depth of the GLF and the height of the ZBCP decrease with increasing Pr concentration.

B. Normalization of the ab-plane data

The low-temperature ab-plane data along with the corresponding numerically calculated backgrounds are shown in Fig. 11(a). The normalized data are shown in Fig. 11(b). The normalized $x=0.0$ and 0.4 data conserve states to better than 1%. The $x=0.2$ data conserve states to better than 10%. The normalized data are also nearly symmetric with respect to energy, as expected for a superconductor.

The data in Fig. 11(b) illustrate the significant new results presented in this article. The data for $x=0.0-0.4$ all exhibit a GLF and a ZBCP. The depth of the GLF and the height of the ZBCP both decrease with increasing Pr concentration. In addition, the energy where the GLF appears decreases with increasing Pr concentration and with the consequent reduction in T_c. The weakening of the GLF and ZBCP and the reduction in the GLF energy are not mere artifacts of the normalization procedure, as this behavior is observed in the unnormalized data too. While different background normalizations yield small changes in the GLF energy, the overall qualitative trend where the GLF energy is observed to decrease with decreasing T_c is not. This correlation between T_c and the GLF energy is an indication that the GLF is related to a superconducting density of states. This also lends support to interpreting the ab-plane conductance in terms of a d-wave density of states at a faceted surface, where the anisotropy between (100)- and (110)-oriented surfaces is erased.[16] Theoretical modeling of these ab-plane tunneling data is in progress and will be reserved for a future publication.

C. Analysis of the low-temperature ab-plane background

This section will analyze the numerically calculated ab-plane background conductance. In order gain better understanding of these data, the low-temperature background conductance is normalized by the actual conductance measured at T_c. This is shown in Figs. 12(a), 12(b), and 12(c) along with low-temperature c-axis tunneling data. These data are normalized by the conductance measured at T_c.

The normalized $x=0.0$ and 0.2 data suggest that the apparent observation of too many states is due to broadly peaked structure over $\sim 15-40$ mV. This structure is temperature dependent and cannot be described by simple thermal broadening effects alone. Interestingly, very similar temperature-dependent structure is observed in the normalized c-axis data. This peaklike structure is also doping dependent. It is most prominent in the undoped data and is virtually absent from the $x=0.4$ and 0.5 data (not shown). Furthermore, it is significant to compare the data from Fig. 12(a) to spectroscopy data measured with a scanning tunneling microscope (STM). The average of STM spectra taken over a 10×10 nm^2 area reveal a broad peaklike structure in

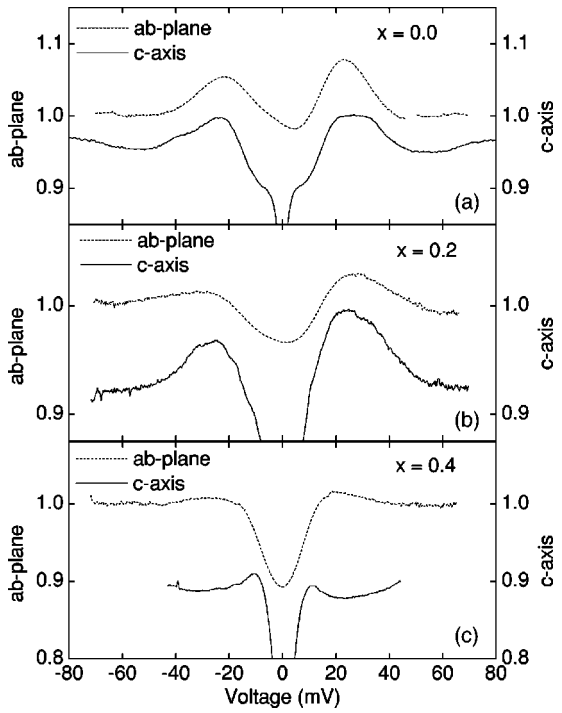

FIG. 12. Comparison of typical high bias structure observed in *c*-axis tunneling and the background conductance used to normalize the low-temperature *ab*-plane data. The low-temperature *c*-axis data and *ab*-plane background conductance are normalized by the conductance measured from the respective junction at T_c. The *c*-axis and *ab*-plane data exhibit very similar temperature-dependent structure over $\sim 15-40$ mV. The different figures correspond to different Pr concentrations. (a) $x=0.0$, (b) $x=0.2$, and (c) $x=0.4$.

the data that is very similar to the peaks observed in planar tunneling.[46] Very similar structure is also found in studies of vortices in YBCO single crystals.[47] Outside the vortex cores, a broad peak followed by a smaller peak at slightly lower energy, reminiscent of the broad peak and GLF of the planar *ab*-plane data, is observed. Inside the cores, the broad peak remains, but the lower energy peak is absent.

The fact that this broad peak is observed in both the *ab*-plane and *c*-axis data, it is doping dependent, and it is observed in experiments with completely different tunnel barriers strongly suggests it is related to the material properties of YPBCO and not due to some barrier effect. Since this peak is most likely the origin of the apparent nonconservation of states and is observed both inside and outside a vortex, this implies that it is unrelated to the superconducting state of YPBCO. It is difficult, however, to specifically say what the physical origin of this peak is. Atomic-scale STM imaging reveals that the copper oxide chains are being probed when this broad peak is observed.[46] But it is unknown whether this is an intrinsic property of the chains or a surface effect. The peak is suppressed at higher temperature more strongly than that expected from simple thermal broadening, suggesting that the peak is sensitive to inelastic scattering. Previous studies also show that this structure is unrelated to T_c. Structure related to this peak in *c*-axis data is observed up to a temperature of 150 K.[48] Our measurements have only been performed up to 90 K, but there are indications for structure related to this peak in our undoped *c*-axis data at this temperature. The suppression of the peak structure with Pr doping implies a sensitivity to disorder within the planes. Beyond these experimental facts, however, no further explanation can be reliably made.

The data in Fig. 12(c) indicate that too few states in the normalized conductance originates from suppression in the conductance around zero bias which develops as the temperature is lowered. The conductance around zero bias decreases with decreasing temperature at a faster rate than that predicted by thermal broadening. The fast decrease in the conductance implies that other transport processes are being frozen out with decreasing temperature. Since the conductance decreases with decreasing temperature, this points toward some type of insulating transport process. The overall temperature dependence is qualitatively consistent with the activation of hopping transport at higher temperature. At high temperature, there is enough thermal energy, in the nature of bosons, to assist the hopping of electrons between localized states in the tunnel barrier. As the temperature is lowered, the bosons are frozen out and elastic, single-step tunneling, which conserves energy and does not require energy from bosons to drive the tunneling process, remains as the only dominant transport process.

Typically, the data from undoped YBCO junctions, when normalized by the conductance measured at T_c, exhibit too many states. The $x=0.2$ data start to show signs of a suppression in the conductance around zero bias. The $x=0.4$ and the $x=0.5$ (not shown) data show clear suppression in the zero-bias conductance with decreasing temperature. The overall behavior is consistent with a thick, amorphous insulating tunnel barrier. The fact that the heavily doped films always have thick amorphous barriers may be related to the material properties of these compounds, but it is most likely not a very profound correlation. The data from undoped films usually exhibit none of this behavior. However, we do occasionally observe too few states in the normalized undoped YBCO conductance. Two examples of this contrasting behavior are shown in Fig. 9. Notice that in the junction exhibiting too few states, there is still evidence for the peak-like structure over $\sim 15-40$ mV. The sum of the data from junctions exhibiting too few states in the normalized data leads to the conclusion that this behavior is related to a barrier effect.

VII. TUNNELING: ANALYSIS OF THE ZBCP FROM YBCO/Cu JUNCTIONS

A. Temperature dependence

The temperature dependence of the ZBCP from YBCO/Cu tunnel junctions[10] will now be discussed. This involves a comparison between data taken at two different temperatures, T_1 and T_2 with $T_1<T_2$. It is crucial to factor out differences in thermal broadening effects in order to make a meaningful comparison between these data. This is accomplished by folding into the low-temperature data the same amount of thermal broadening that is present in the higher-temperature data. The low-temperature data are numerically convolved with the derivative of the Fermi function with respect to voltage evaluated at a temperature $T_{conv}=T_2$. Since the low-temperature data inevitably have finite thermal broadening, the convolved data are only an

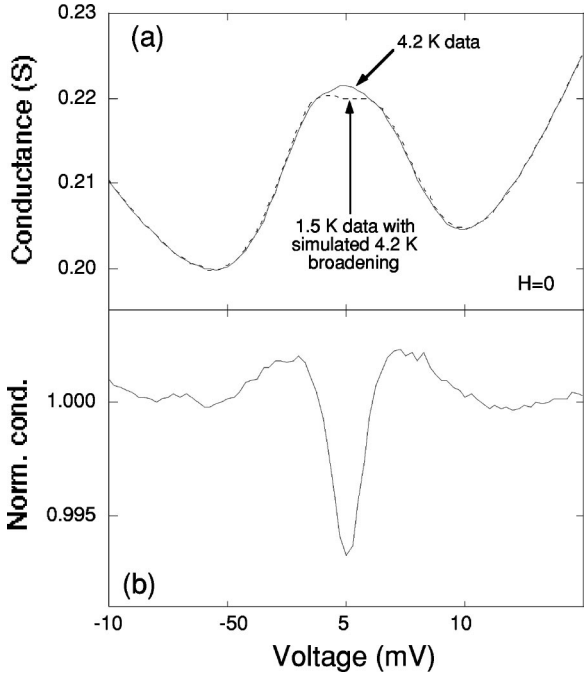

FIG. 13. Temperature dependence of the ZBCP in zero magnetic field. (a) A comparison of actual data measured at 4.2 K to data measured at 1.5 K that are numerically convolved with 4.2 K thermal broadening. Note that the curves do not match, indicating a temperature-dependent density of states. (b) Normalization of the convolved 1.5 K data by the actual 4.2 K data from (a). Spectral weight is shifted away from zero bias into the finite energy peaks at $\sim \pm 2$ mV. Compare these data to the field-dependent data shown in Fig. 16.

approximation. But this approximation is good if T_1 is close to 0 K so that the data have minimal thermal broadening. As a check on the accuracy of this approximation, comparisons are also made between actual data measured at T_2 and simulated 0 K data that are convolved with T_2 thermal broadening. The simulated 0 K data are generated by deconvolving 1.5 K thermal broadening from data measured at 1.5 K. The deconvolution routine is the same as that described above. The results of the analysis are qualitatively the same, regardless of whether the numerical data with T_2 broadening are generated from actual 1.5 K data or from the simulated 0 K data. Only slight quantitative differences are observed, which are stated below. For simplicity, only those data that are calculated by starting from the actual 1.5 K data are presented.

When the ZBCP splits in zero magnetic field, the temperature dependence cannot be described by thermal broadening effects alone. An example of this analysis is shown in Fig. 13(a). Data taken at 1.5 K are convolved with 4.2 K thermal broadening. The numerically generated data do not match the actual data measured at 4.2 K. Similar results are observed when comparing to 7.5 K and 10 K data. Thus, the density of states is temperature dependent. The observed temperature dependence exhibits the same qualitative behavior expected when measuring a feature related to the superconducting density of states. As the temperature is lowered, spectral weight is shifted from zero bias into two peaks at $\sim \pm 2$ mV, as shown in Fig. 13(b). Over ± 10 mV, the total integrated area with respect to the 4.2 K data is approximately 10% of the area above and below the 4.2 K curve, implying a rough conservation of states. When the normalization is performed using numerical data generated from the simulated 0 K data, the conservation of states is approximately 20%. This is important because conservation of states must be observed before interpreting the data in terms of an Andreev bound state of *d*-wave superconductors. Data beyond 10 mV are unreliable because there are sharp jumps that have all the hallmarks of noisy contacts and are unrelated to any material properties being studied. However, it is expected that this is beyond the energy range over which the bound-state splitting will have an effect on the density of states.

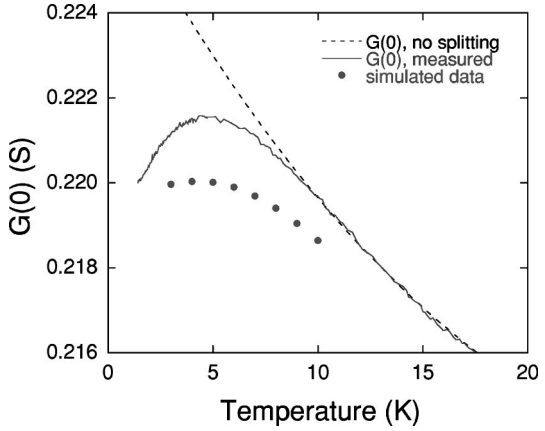

FIG. 14. Comparison of the actual temperature dependence of the zero-bias conductance $G(0)$ to the zero-bias conductance determined by numerically convolving the 1.5 K conductance with thermal broadening. The dotted line is the expected temperature dependence of $G(0)$ when there is no splitting in the density of states, as discussed in the text.

More evidence for a temperature-dependent density of states comes from an analysis of the zero-bias conductance $G(0)$ versus temperature. The ZBCP appears in the conductance well below T_c. Here $G(0)$ begins to increase at roughly this same temperature and continues to increase until the Andreev bound state splits, leading to a downturn in $G(0)$ as the temperature goes to zero. Note that this cannot be ascribed to overall shifts in the background conductance since it stays constant over this temperature range. If the 1.5 K data (or the simulated 0 K data) are numerically convolved with higher-temperature thermal broadening, the numerically generated data do not match the measured $G(0)$. This is shown in Fig. 14. The splitting in the density of states pulls $G(0)$ down below the value it would have if there were no splitting.

The temperature dependence of $G(0)$ is also used to determine the onset of splitting in the density of states. Because of thermal broadening effects, a splitting in the density of states at a temperature T_s can only be resolved in the conductance well below this temperature. Therefore, $G(0)$ provides a more accurate measure of T_s. This involves comparing the measured temperature dependence of $G(0)$ to some expected temperature dependence when there is no splitting of the Andreev bound state. Theoretical calculations show that a ZBCP resulting from an Andreev bound state should exhibit a T^{-1} temperature dependence.[18] The experimental data can be fit to this functional form over a limited tempera-

ture range, but the overall fit is poor because the T^{-1} prediction ignores the finite width of the bound state observed in practice and the contribution of the GLF to the thermal broadening effects. Numerical convolutions of both experimental data and theoretical curves, which include a GLF and an impurity-broadened ZBCP,[49] yield $G(0)$ vs T curves that deviate from the T^{-1} behavior. We instead prefer to compare our data to numerically determined temperature dependence. This temperature dependence is generated by convolving data from a YBCO/Pb junction at 4.2 K in a 2 kG magnetic field with thermal broadening and extracting $G(0)$ vs T. This is shown as a dotted line in Fig. 14. The definition of T_s is where the measured data deviate from the expected temperature dependence. Finally, $G(0)$ can also be fit to the $\log(1/T)$ dependence expected from magnetic spin-flip scattering. But, the temperature range over which the data agree is too limited to draw any definitive conclusions.

Last, the ZBCP is always observed below the T_c of the film under study. This in itself is consistent with, but not rigorous proof, of its interpretation as an Andreev bound state. Since the width, in energy, of the ZBCP is much less than the thermal energy at T_c, $k_B T_c$, the ZBCP is impossible to resolve at T_c, even if it is temperature independent. But the ZBCP in undoped YBCO films is sometimes observed above 45 K, which is the T_c of the YPBCO-40% films. In contrast, the ZBCP in YPBCO-40% films is never observed above 25 K.

B. Magnetic field dependence

The YBCO ZBCP splits when an external magnetic field is applied to the tunnel junction. This same qualitative behavior is also observed when a ZBCP originates from magnetic spin-flip scattering in the insulating tunnel barrier.[50] This is the reason why the YBCO ZBCP was originally interpreted[5] using the spin-flip scattering model.[51] But it was acknowledged that there were some discrepancies. In Fig. 7 of Ref. 5, the splitting versus field is nonlinear and much larger than the expected Zeeman splitting of ordinary paramagnetic spins. A direct comparison to representative experimental data from spin-flip ZBCP's (Refs. 50, 52–54, and 56) shows dramatic, qualitative differences between the YBCO and spin-flip data. This is shown in Fig. 15, where the peak position is plotted as a function of magnetic field. The voltage at which the conductance reaches a maximum is used to determine the peak position. The peak position plotted in Fig. 15 is an average of the absolute value of the peak position voltage for positive and negative bias. With the exception of the $Sn/Sn_xO_y/Sn$ junction data, the magnetic impurity data are clustered around each other and obey a roughly linear variation of peak position versus field. Other published data from junctions with paramagnetic impurities[55,57,58] are also clustered around the linear data, but have been omitted from Fig. 15 for clarity.

For the YBCO data below 1 T, the slope of peak position versus field is much larger than the slope of the spin-flip data. The slope of the $Ta/Ta_2O_5/Al$ data[50] is 0.118 meV/T while the slope below 1 T for the YBCO/Pb (Ref. 5) and YBCO/Cu (Ref. 10) data is 0.753 and 0.771 meV/T, respectively. Assuming the Zeeman energy $g\mu_B H$ sets the energy scale for the splitting, the slope of the curves in Fig. 15 yields $g\mu_B$ (where g is the Landé g factor, μ_B is the Bohr magneton, and H is the magnetic field). The slope of the $Ta/Ta_2O_5/Al$ data yields a Landé g factor of $g \sim 2$, which is a reasonable and realistic value for the proposed Ta impurities in the tunnel barrier. The slopes from the YBCO data imply an enormous Landé g factor of $g \sim 13$. This is in contradiction to any physically realistic interpretation of the ZBCP in terms of paramagnetic spins.

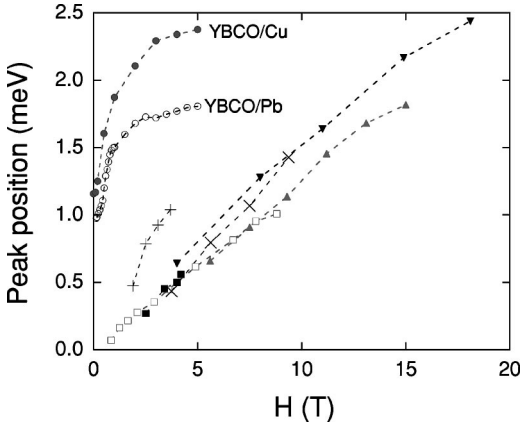

FIG. 15. A compendium of experimental data comparing and contrasting the peak position vs magnetic field of the YBCO ZBCP to ZBCP's originating from magnetic spin-flip scattering. The data from planar YBCO junctions are labeled accordingly. Data from junctions with magnetic impurities in the barrier are represented by (□) for $Ta/Ta_2O_5/Al$ (Ref. 50), (■) for Al/Ti-doped Al_2O_3/Al (Ref. 52), (▲) for Al/Ti-doped Al_2O_3/Al (Ref. 53), (▼) for Al/Fe-doped Al_2O_3/Al (Ref. 54), (+) for $Sn/Sn_xO_y/Sn$ (Ref. 55), and (×) for a Au/Si:P Schottky barrier tunnel junction (Ref. 56).

This large slope, however, is easily accounted for by the d-wave Andreev bound-state model. Supercurrents induced by an external magnetic field will shift the bound state to finite energy. Reasonable values of the thermodynamic critical field and tunneling cone of 0.94 T and 3°, respectively, yield a slope that agrees very well with the large slope of the YBCO data in Fig. 15.[10,16] Furthermore, when the effects of a subdominant order parameter, nonlinearity in the screening current, and the bulk thermodynamic critical current are taken into account, the finite splitting at zero field and the nonlinearity in the peak position vs field are well described by the d-wave model.

Typical field-dependent data are shown in Fig. 16(a). Application of a field induces further splitting of the peak. Note that, like the behavior with decreasing temperature, application of a field shifts spectral weight from the region around zero bias, out to finite voltage. The finite field data are normalized by the zero field data in Fig. 16(b). Note that all the data in Fig. 16(a) are taken at the same temperature, so there are no differences in thermal broadening. The data in Fig. 16(b), like the normalized data in Fig. 13(b), exhibit a rough conservation of states. Again, this is the expected behavior from a feature related to the superconducting density of states. Between ± 8 mV, the total integrated area with respect to the zero-field data is approximately 10% of the area above and below the zero field reference curve. The low-field data have more states than the zero-field spectrum while the high-field data have less. The normalized data in large fields undershoots the zero-field data for voltages beyond 8 mV

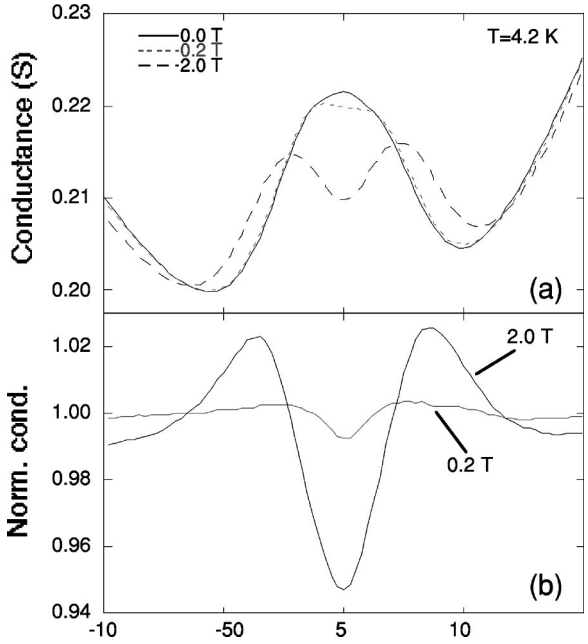

FIG. 16. Magnetic field dependence of the ZBCP. (a) Data taken at 4.2 K in different applied magnetic fields, as indicated. The application of a magnetic field induces the ZBCP to split. (b) Normalized magnetic field-dependent data. As the field increases, spectral weight is shifted from zero bias into finite energy peaks. Compare these data to the temperature-dependent data shown in Fig. 13.

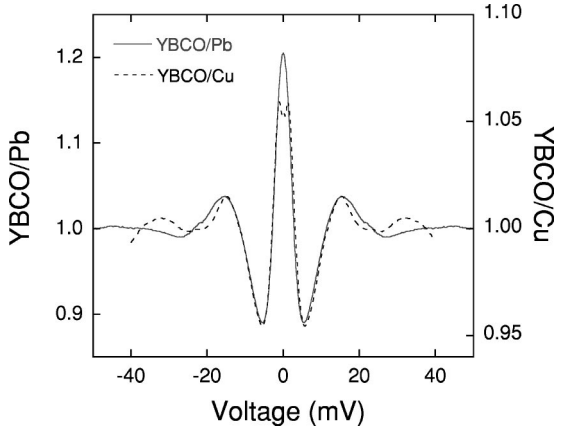

FIG. 17. Comparison of the normalized even conductance from ab-oriented YBCO films with Pb and Cu counterelectrodes. Note the differences in the vertical scales for the 2 sets of data. Both sets exhibit a GLF at the same energy, but the depth of the GLF in the YBCO/Cu data is more than a factor of 2 less than the depth of the YBCO/Pb GLF.

and persists out to the GLF energy. Integration over a larger energy range results in poorer conservation of area. This undershoot is barely discernible in the low-field data, but gets progressively larger with increasing magnetic field. It remains unclear whether this behavior is related to the density of states or whether it is some effect acting independently of the spectral shifts associated with the Andreev bound state.

It is significant to compare the normalized data in Fig. 13(b) to the normalized data in Fig. 16(b). Decreasing the temperature from 4.2 K to 1.5 K produces almost the same change in the conductance as applying a 2 kG magnetic field at 4.2 K. This similarity provides further support of the Andreev bound-state interpretation of the YBCO ZBCP and is a convincing sign that the zero-field splitting originates from the spontaneous generation of supercurrent. Specifically, the bound state shifts to finite energy whenever there is a finite superfluid momentum, regardless of whether the superfluid circulation is induced by an external magnetic field or spontaneously by the formation of two order parameters with a relative $\pi/2$ phase difference.

C. Comparison of the GLF's from YBCO/Cu and YBCO/Pb junctions

The last feature we wish to identify is the smaller depth of the GLF from YBCO/Cu junctions compared to YBCO/Pb junctions. To make a quantitative comparison, the background conductance must first be divided out. Representative YBCO/Cu and YBCO/Pb data are normalized according to the same numerical procedure, as described above, and shown in Fig. 17. To eliminate the slight asymmetry with respect to voltage in the normalized data, the even conductance is calculated. The even conductance is simply an average of the conductance at positive and negative voltage, $G_{even}(V) \equiv [G(+V)+G(-V)]/2$. The variation in the normalized YBCO/Cu conductance for $V>30$ mV is an artifact of the normalization and should be ignored. The depth of the GLF from YBCO/Cu junctions is reproducibly less than the depth of the GLF from YBCO/Pb junctions. Similar behavior is also observed in Pr-doped YBCO/Pb junctions, where the depth of the GLF decreases when the Pr concentration increases. Damage induced by ion irradiation, which increases the disorder in the YBCO film, also yields a GLF that is shallower.[59] Using this phenomenological behavior as a guide, YBCO/Cu junctions apparently have more disorder and quasiparticle scattering near the tunnel barrier compared to the YBCO/Pb junctions.

VIII. CONCLUSION

In conclusion, the resistivity along the copper oxide planes and the quasiparticle tunneling conductance of YPBCO thin films are studied. The YPBCO in-plane resistivity exhibits features that are common to both planar and chain substitutions in YBCO. Doping YBCO with Pr introduces a large extrapolated zero-temperature residual resistivity, characteristic of planar doping, and S-shaped curvature in the temperature dependence, characteristic of chain doping. The resistivity shows signs of carrier localization around the Fermi energy before undergoing a superconductor-insulator transition. The localization foreshadows the variable-range hopping transport observed in insulating PBCO. The sheet resistance per copper oxide bilayer at the superconductor-insulator transition is approximately equal to the quantum resistance for Cooper pairs, $R_Q = h/(2e)^2 \sim 6.45\ \mathrm{k}\Omega$.

The planar quasiparticle tunneling conductance exhibits a clear dependence on crystallographic orientation and Pr concentration. Tunneling into c-axis films is qualitatively different than tunneling into ab-oriented films. This crystallographic dependence persists for all four Pr doping levels studied. The ab-plane data for $x \leqslant 0.4$ exhibit a gaplike feature and a zero-bias conductance peak, which are qualitatively consistent with a d-wave symmetry superconductor at

an ab-oriented surface with nm-scale faceting. The GLF energy decreases when T_c is suppressed by Pr doping, and the GLF depth and the ZBCP height decrease with increasing impurity scattering. Finally, the temperature and magnetic field dependence of the ZBCP agrees with predictions for a surface Andreev bound state from a d-wave superconductor. Analysis indicates that states are conserved to within 10%, which is consistent with a feature of a superconducting density of states. The same qualitative behavior is observed either when the ZBCP splits spontaneously in zero magnetic field or when it splits in an external magnetic field.

c-axis tunneling data exhibit a conductance dip at zero bias, in contrast to the ab-plane ZBCP, and a broad, temperature- and doping-dependent peak over $\sim 15-40$ mV. The broadly peaked structure gets weaker but does not shift in energy with doping, which is different from the ab-plane GLF. However, there is evidence that this broadly peaked structure appears in the ab-plane conductance too. This broad peak coincides at roughly the same energy as the ab-plane GLF for undoped YBCO only. Finally, the background conductance is qualitatively different between the two orientations.

ACKNOWLEDGMENTS

It is a pleasure to acknowledge many stimulating conversations with M. Fogelström, D. Rainer, and J. A. Sauls. We would also like to acknowledge helpful and interesting discussions with M. Aprili and J. M. Rowell. The self-assembled monolayers on YBCO were developed by C. A. Mirkin, F. Xu, and J. Zhu. We are additionally grateful to J. Giapintzakis for performing SQUID measurements on some of our films and to W. L. Feldmann for technical support. This research was supported by the Science and Technology Center for Superconductivity through National Science Foundation Grant No. NSF DMR 91-20000. Materials characterizations were performed at the Center for Microanalysis of Materials at the Frederick Seitz Materials Research Laboratory, University of Illinois at Urbana-Champaign, Grant No. DE FG 02-96ER45439.

*Present address: Seagate Technology, Pittsburgh, PA 15203-2116.

[1] W. L. McMillan and J. M. Rowell, in *Superconductivity*, edited by R. D. Parks (Marshall-Dekker, New York, 1969), Vol. 1, p. 561.
[2] A. Fournel, I. Oujia, J. P. Sorbier, H. Noel, J. C. Levet, M. Potel, and P. Gougen, Europhys. Lett. **6**, 653 (1988).
[3] J. Geerk, X. X. Xi, and G. Linker, Z. Phys. B: Condens. Matter **73**, 329 (1988).
[4] M. Gurvitch, J. J. M. Valles, A. M. Cucolo, R. C. Dynes, J. P. Garno, L. F. Schneemeyer, and J. V. Waszcak, Phys. Rev. Lett. **63**, 1008 (1989).
[5] J. Lesueur, L. H. Greene, W. L. Feldmann, and A. Inam, Physica C **191**, 325 (1992).
[6] D. J. Van Harlingen, Rev. Mod. Phys. **67**, 515 (1995).
[7] R. Di Leo, A. M. Cucolo, A. Nigro, P. Romano, and F. Licci, Solid State Commun. **92**, 873 (1994).
[8] A. G. Sun, L. M. Paulius, D. A. Gajewski, M. B. Maple, and R. C. Dynes, Phys. Rev. B **50**, 3266 (1994).
[9] A. M. Cucolo, R. C. Dynes, J. J. M. Valles, and L. F. Schneemeyer, Physica C **179**, 69 (1991).
[10] M. Covington, M. Aprili, E. Paraoanu, L. H. Greene, F. Xu, J. Zhu, and C. A. Mirkin, Phys. Rev. Lett. **79**, 277 (1997).
[11] L. J. Buchholtz and G. Zwicknagl, Phys. Rev. B **23**, 5788 (1981).
[12] C.-R. Hu, Phys. Rev. Lett. **72**, 1526 (1994); J. Yiang and C.-R. Hu, Phys. Rev. B **50**, R16 766 (1994).
[13] Y. Tanaka and S. Kashiwaya, Phys. Rev. Lett. **74**, 3451 (1995).
[14] M. Matsumoto and H. Shiba, J. Phys. Soc. Jpn. **64**, 1703 (1995); *ibid.* **64**, 4867 (1995).
[15] L. J. Buchholtz, M. Palumbo, D. Rainer, and J. A. Sauls, J. Low Temp. Phys. **101**, 1099 (1995).
[16] M. Fogelström, D. Rainer, and J. A. Sauls, Phys. Rev. Lett. **79**, 281 (1997).
[17] Y. S. Barash, A. A. Svidzinsky, and H. Burkhardt, Phys. Rev. B **55**, 15 282 (1997).
[18] A. F. Andreev, Zh. Éksp. Teor. Fiz. **46**, 1823 (1964) [Sov. Phys. JETP **19**, 1228 (1964)].
[19] M. Atiyah, V. Patodi, and I. Singer, Proc. Cambridge Philos. Soc. **77**, 43 (1975).
[20] L. H. Greene, B. G. Bagley, W. L. Feldmann, J. B. Barner, F. Shokoohi, P. Miceli, A. Fathy, D. Kalokitis, and V. Pendrick, Appl. Phys. Lett. **59**, 1629 (1991).
[21] M. Covington, R. Scheuerer;, K. Bloom, and L. H. Greene, Appl. Phys. Lett. **68**, 1717 (1996).
[22] N. F. Mott, *Metal-Insulator Transitions* (Taylor & Francis, London, 1974).
[23] W. F. Brinkman, R. C. Dynes, and J. M. Rowell, J. Appl. Phys. **41**, 1915 (1970).
[24] S.-W. Han, J. A. Pitney, P. F. Miceli, M. Covington, L. H. Greene, M. J. Godbole, and D. H. Lowndes, Physica B **221**, 235 (1996).
[25] R. G. Nuzzo and D. L. Allara, J. Am. Chem. Soc. **105**, 4481 (1983).
[26] K. Chen, C. A. Mirkin, R.-K. Lo, J. Zhao, and J. T. McDevitt, J. Am. Chem. Soc. **117**, 6374 (1995).
[27] H. B. Radousky, J. Mater. Res. **7**, 1917 (1992).
[28] J. J. Neumeier and M. B. Maple, Physica C **191**, 158 (1992).
[29] W. Jiang, J. L. Peng, S. J. Hagen, and R. L. Greene, Phys. Rev. B **46**, 8694 (1992).
[30] T. R. Chien, Z. Z. Wang, and N. P. Ong, Phys. Rev. Lett. **67**, 2088 (1991).
[31] D. J. C. Walker, A. P. Mackenzie, and J. R. Cooper, Phys. Rev. B **51**, 15 653 (1995).
[32] Y. Fukuzumi, K. Mizuhashi, K. Takenaka, and S. Uchida, Phys. Rev. Lett. **76**, 684 (1996).
[33] T. Ito, K. Takenaka, and S. Uchida, Phys. Rev. Lett. **70**, 3995 (1993).
[34] A. Carrington, A. P. Mackenzie, C. T. Lin, and J. R. Cooper, Phys. Rev. Lett. **69**, 2855 (1992).
[35] B. Moeckly and K. Char, Physica C **265**, 283 (1996).
[36] Y. Suzuki, J.-M. Triscone, C. B. Eom, M. R. Beasley, and T. H. Geballe, Phys. Rev. Lett. **73**, 328 (1994).
[37] R. Meservey and B. B. Schwartz, in *Superconductivity*, edited by R. D. Parks (Marcel Dekker, New York, 1969), p. 117.
[38] P. W. Anderson and Z. Zou, Phys. Rev. Lett. **60**, 132 (1988).
[39] J. R. Kirtley and D. J. Scalapino, Phys. Rev. Lett. **65**, 798 (1990).
[40] P. B. Littlewood and C. M. Varma, Phys. Rev. B **45**, 12 636 (1992).
[41] D. A. Wollman (private communication).

[42] M. Covington, F. Xu, C. A. Mirkin, W. L. Feldmann, and L. H. Greene, Czech. J. Phys. **46**, 1341 (1996).
[43] W. Jiang, J. L. Peng, J. J. Hamilton, and R. L. Greene, Phys. Rev. B **49**, 690 (1994).
[44] U. Kabasawa, Y. Tarutani, M. Okamoto, T. Fukazawa, A. Tsukamoto, M. Hiratani, and K. Takagi, Phys. Rev. Lett. **70**, 1700 (1993).
[45] R. C. Dynes, J. P. Garno, G. B. Hertel, and T. P. Orlando, Phys. Rev. Lett. **53**, 2437 (1984).
[46] H. L. Edwards, D. J. Derro, A. L. Barr, J. T. Markert, and A. L. de Lozanne, Phys. Rev. Lett. **75**, 1387 (1995).
[47] I. Maggio-Aprile, C. Renner, A. Erb, E. Walker, and Ø. Fischer, Phys. Rev. Lett. **75**, 2754 (1995).
[48] J. Geerk, G. Linker, O. Meyer, F. Ratzel, and R. Smithey, in *Tunneling Phenomena in High and Low Tc Superconductors*, edited by A. di Chiara and M. Russo (World Scientific, Singapore, 1993), p. 1.
[49] M. Fogelström, J. A. Sauls, M. Covington, M. Aprili, and L. H. Greene (unpublished).
[50] J. A. Appelbaum and L. Y. L. Shen, Phys. Rev. B **5**, 544 (1972).
[51] J. A. Appelbaum, Phys. Rev. **154**, 633 (1967).
[52] D. J. Lythall and A. F. G. Wyatt, Phys. Rev. Lett. **20**, 1361 (1968).
[53] P. Nielsen, Phys. Rev. B **2**, 3819 (1970).
[54] S. Bermon, D. E. Paraskevopoulos, and P. M. Tedrow, Phys. Rev. B **17**, 2110 (1978).
[55] L. Y. L. Shen and J. M. Rowell, Phys. Rev. **165**, 566 (1968).
[56] E. L. Wolf and D. L. Losee, Phys. Rev. B **2**, 3660 (1970).
[57] S. Gregory, Phys. Rev. Lett. **68**, 2070 (1992).
[58] D. C. Ralph and R. A. Buhrman, Phys. Rev. Lett. **72**, 3401 (1994).
[59] M. Aprili, M. Covington, E. Paraoanu, B. Niedermeier, and L. H. Greene, Phys. Rev. B **57**, R8139 (1998).